magnetochemistry

MDPI

Supplementary Materials

Structural and Photocatalytic Studies on Oxygen Hyperstoichiometric Titanium-Substituted Strontium Ferrite Nanoparticles

Jaspreet Kaur Grewal [1], Manpreet Kaur [1,*], Rajeev K. Sharma [2], Aderbal C. Oliveira [3], Vijayendra Kumar Garg [3] and Virender K. Sharma [4,*]

[1] Department of Chemistry, Punjab Agricultural University, Ludhiana 141001, Punjab, India
[2] Department of Physics, Punjab Agricultural University, Ludhiana 141001, Punjab, India
[3] Institute of Physics, University of Brasilia, Brasilia 70000-000, Brazil
[4] Program for Environment and Sustainability, Department of Environmental and Occupational Health, School of Public Health, Texas A&M University (TAMU), College Station, TX 77843-1266, USA
* Correspondence: manpreetchem@pau.edu (M.K.); vsharma@tamu.edu (V.K.S.)

Citation: Grewal, J.K.; Kaur, M.; Sharma, R.K.; Oliveira, A.C.; Garg, V.K.; Sharma, V.K. Structural and Photocatalytic Studies on Oxygen Hyperstoichiometric Titanium-Substituted Strontium Ferrite Nanoparticles. *Magnetochemistry* **2022**, *8*, 120. https://doi.org/10.3390/magnetochemistry8100120

Academic Editor: Lotfi Bessais

Received: 6 August 2022
Accepted: 28 August 2022
Published: 6 October 2022

Publisher's Note: MDPI stays neutral with regard to jurisdictional claims in published maps and institutional affiliations.

Text S1

Characterization techniques

The magnetic properties of the synthesized $Sr_{1-x}Ti_xFe_2O_{4+\delta}$ (x = 0.0, 0.3, 0.6 & 1.0) were determined by vibrating sample magnetometer (VSM Model, PAR-155). XRD, Panlytical X'pert Pro with Cu Kα radiations (λ = 1.5404 A^{o}) was used to determine the phase constitutes of the fabricated catalysts. The micromorphology of the obtained powders were detected by TEM model Hitachi Hi-7650 and SEM model Hitachi S-3400 whereas the EDX images were recorded on thermo Noran System utilizing point and shoot method. Quantachrome Nova-1000 was used to carry out the nitrogen adsorption-desorption experiments and BET (Brunauer-Emmett-Teller) specific surface area of the fabricated ferrites was determined based on the obtained isotherm data. Dynamic light scattering and zeta potential analysis were recorded by using Zetasizer Nano- ZS to determine particle size distribution and stability of colloidal dispersions. FT-IR measurements were carried out on FT-IR Spectrophotometer (Perkin Elmer, Model RX-1) using KBr pellets, in the wave number ranging between 4000-400 cm^{-1}. Agilent Cary Eclipse Fluorescence spectrophotometer was used to record fluorescence spectra. The residual concentration of *p*-nitrophenol, pendimethalin and martius yellow solutions were determined by UV-visible spectrophotometer (UV-1800 Shimadzu UV-visible) at wavelengths of 398, 465 and 445 nm, respectively. The Mössbauer spectra of the samples were noted with transducer (Wissel) coupled to ^{57}Co in Rh matrix source in the conventional transmission geometry. Al/$Sr_{1-x}Ti_xFe_2O_{4+\delta}$ (x = 0.0, 0.3, 0.6 & 1.0) ferrite nanoparticles schottky diode is obtained and the Hioki LCR HiTester (Model no. 3532-50) was used for the measurements of Capacitance-Voltage. Operating frequencies for the HIOKI 3522-50 LCR tester ranges from 1 mHz to 100 KHz. Automatic bridge balance technique is used by the tester. Silver serves as the top electrode, while the aluminium substrate serves as the bottom electrode. The top electrode is made from the high quality conducting silver paste. The degradation of organic pollutants and evolution of their hydroxylated intermediates and end products were also monitored by gas chromatography-mass spectrometry (Thermo Scientific TSQ 8000 Gas Chromatograph - Mass Spectrometer).

Text S2

Oxygen content

The iodometric titration [35] was adopted to evaluate the non-stochiometry (δ) in $Sr_{1-x}Ti_xFe_2O_{4+\delta}$ (x = 0.0 -1.0). The sample powders were dried in an oven at 100℃ for 1 hour to eliminate the moisture content and adsorbed gases. Accurately weighed (500 mg) the samples and dissolved in 1 M HCl solution (100 mL). 2.0 g of KI was added into the solutions.

The sample solutions were then titrated with the $Na_2S_2O_3$ solution using starch as an indicator. The endpoint appeared with the disappearance of blue color. The volume consumed of $Na_2S_2O_3$ is recorded as V and δ value was determined using following Equation.

$$\delta = \frac{Mo - \frac{m}{C.V}}{\frac{2m}{C.V} - Moxy}$$

Where M_O represents the molecular weight of the $Sr_{1-x}Ti_xFe_2O_{4+\delta}$ (x = 0.0 -1.0) samples, m defines the weight of powdered samples, C refers to the the molar concentration of $Na_2S_2O_3$ solution (0.001 M) and M_{Oxy} represents the weight of oxygen atom.

Text S3

Zeta potential measurements

For zeta (ξ) potential measurements, 1.0 N NaOH and 1.0 N HCl were poured into the flasks containing 30.0 mL of deionized water to adjust the pH to 1.0, 3.0, 6.0 and 9.0. Then, 2.0 mg of ferrite NPs was added to solution (2.0 mL) of each pH. The ξ-potential of the solutions (0.8 mL) was determined using ξ- potential analyzer and was plotted against different pH values (Fig. 7b).

Text S4

Limits of detection and Quantification

The values of limit of detection (LOD) and quantification (LOQ) for *p*-nitrophenol, pendimethalin and martius yellow solutions were evaluated as:

$$LOD = 3\ (s/S)$$

$$LOQ = 10\ (s/S)$$

Here, S = slope of the calibration curve and s = standard deviation of replicate measurements having lowest concentration in the calibration curve.

For the present work, the respective LOD values for and LOQ values for *p*-nitrophenol, pendimethalin and martius yellow solutions were determined to be 6.01×10^{-3}, 1.3×10^{-3} and 1.01×10^{-3} mg/L, respectively. LOQ values were found to be 1.96×10^{-2}, 4.3×10^{-3} and 3.36×10^{-3} for *p*-nitrophenol, pendimethalin and martius yellow, respectively.

Text S5

Determination of chemical oxygen demand (COD)

The chemical oxygen demand (COD) represents the oxygen consumed in water by biologically degradable and inert matter during chemical oxidation. The higher value of COD implies the reduction of dissolved oxygen levels due to presence of large amount of oxidizable organic matter in sample. For determining COD levels, 15 mL of conc. H_2SO_4 and 5 mL of 0.25 N $K_2Cr_2O_7$ were added to 20 mL of samples. These samples were collected in hard digestion tubes, sealed with cellulose caps and placed in autoclave for digestion. After 30-45 mins, the sample was titrated with ferrous ammonium sulfate ($FeSO_4(NH_4)_2SO_4$) until the red end point was reached, with Ferroin as an indicator. The blank samples containing reagents and distilled/ground water were also titrated by similar procedure. The formula used for evaluating COD is as follows:

$$\text{COD} = \frac{(\text{A}-\text{B})\text{C} \times 8 \times 1000}{\text{Volume of Sample}}$$

$$\text{COD} = \frac{(\text{A}-\text{B}) \times 0.25 \times 8 \times 1000}{\text{Volume of Sample}}$$

$$COD = (A\text{-}B) \times 100$$

Where A is volume of $FeSO_4(NH_4)_2SO_4$ used for the blank
B is the volume of $FeSO_4(NH_4)_2SO_4$ used for the sample
C is normality of $FeSO_4(NH_4)_2SO_4$ solution used.

Text S6

C-V measurement

A thin film Al/ $Sr_{1-x}Ti_xFe_2O_{4+\delta}$ (x = 0.0, 0.3, 0.6 & 1.0) ferrite nanoparticles schottky diode was fabricated. The performance of schottky diode is drastically influenced by the interface properties of metal-semiconducting contacts. The barrier height (Φ_b) of schottky diode is crucial factor in determining the width of depletion region of semiconductor. The present study was carried out to calculate capacitance-voltage parameters *viz.* built-in voltage (V_{bi}), carrier concentration (N_D) and barrier height (Φ_b) and the equations used for evaluating the C-V parameters are listed in Table S1. C-V measurements utilises a Schottky barrier junction to generate a region that lacks the conducting electrons and holes, defined as depletion region. This zone contains electrically active defects and ionized donors and contributes towards the capacitive performance. With the determination of numerous C-V measurement parameters, a great deal of knowledge regarding the properties of semiconductors can be acquired.

Table S1. Equations used for the determination of C-V parameters.

Depletion layer capacitance (C)	$\boldsymbol{C = \frac{dQ_{SC}}{dV} = \sqrt{\frac{q\varepsilon_S A^2 N_D}{2(V_{bi}+V)}} = \frac{\varepsilon_S}{W}}$
Carrier concentration (N_D)	$\frac{1}{C^2} = \frac{2(V_{bi}-V)}{q\varepsilon_S A^2 N_D}$
Barrier height (Φ_b)	$\varphi_b = V_{bi} + V_n$
Gap between the top of conduction band and fermi level (V_n)	$V_n = \frac{KT}{q}\ln\left(\frac{N_C}{N_D}\right)$
Acceptor concentration (N_C)	$N_C = 2\left(\frac{2\pi mKT}{h^2}\right)^{3/2}$

Where dQ_{SC} = Increased change of charge with the increased change in voltage dV, N_D = Carrier concentration, A = Area of Schottky diode, ε_s = Electrical permittivity of the prepared samples, V_{bi} = Built-in voltage, K = Boltzman's constant, h = Planck's constant, T = Temperature, m = Mass of electron, N_C = Acceptor concentration

Text S7

Influence of catalyst dose

In case of *p*-nitrophenol, pendimethalin and martius yellow, the catalyst dose of $Sr_{0.4}Ti_{0.6}Fe_2O_{4.6}$ NPs was varied from 0.02 g/L to 1.0 g/L at the optimized pH of 3.0. It was observed that rate of photodegradation increased proportionally with the amount of catalyst added upto 0.2 g/L for *p*-nitrophenol and pendimethalin and 0.4 g/L for martius yellow due to the increased number of active photocatalytic sites. But afterwards, a drop in the photocatalytic rate achieved at higher catalyst loading due to the increased tendency towards aggregation i.e. particle-particle interaction also increased because of decrease in the surface area accessible for absorption of light. Moreover, the high frequency of $Sr_{0.4}Ti_{0.6}Fe_2O_{4.6}$ photocatalyst crumbs floating in the solutions of nitroaromatic contaminants solution prevented the penetration of visible light. And due to this, no more light could enter onto the surface of photocatalyst as the surrounding granules would provide shade onto their surface (Wu and Zhang 2019). Hence, the lesser penetration of light led to reduced exposure area and consequently resulted into reduced photoactivity. The comparative photocatalytic degradation of martius yellow, *p*-nitrophenol and pendimethalin

using $Sr_{0.4}Ti_{0.6}Fe_2O_{4.6}$ NPs is presented in Fig. 6 f. It was observed that $Sr_{0.4}Ti_{0.6}Fe_2O_{4.6}$ NPs displayed the maximum (%) photodegradation efficiency of 86.4 % for martius yellow at 0.4 g/L of catalyst dose, 91.5 and 93.8 % for *p*-nitrophenol and pendimethalin at 0.2 g/L of catalyst dose.

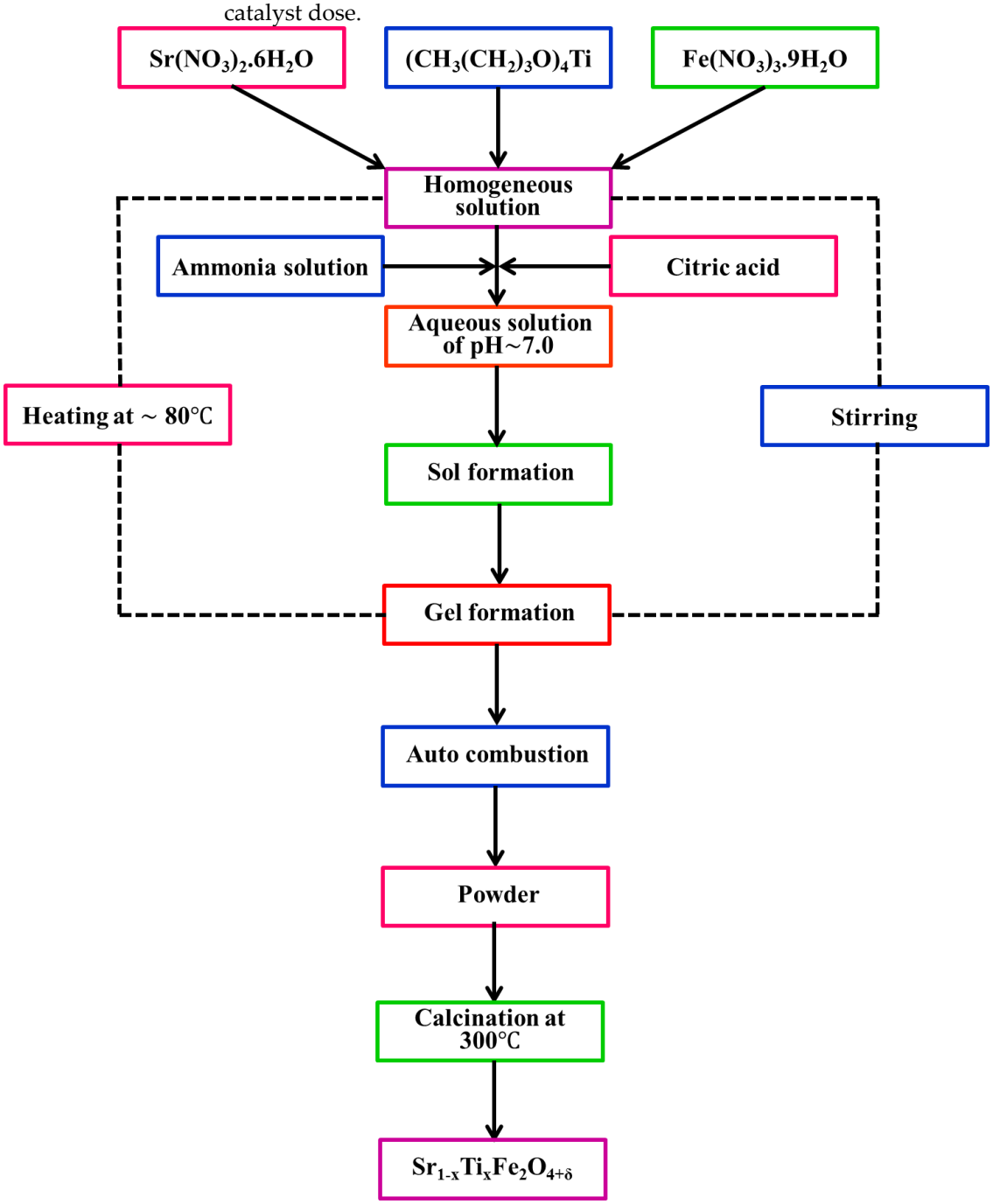

Scheme S1. Schematic representation of synthesis of oxygen hyperstoichiometric trimetallic titanium substituted strontium ferrite nanoparticles.

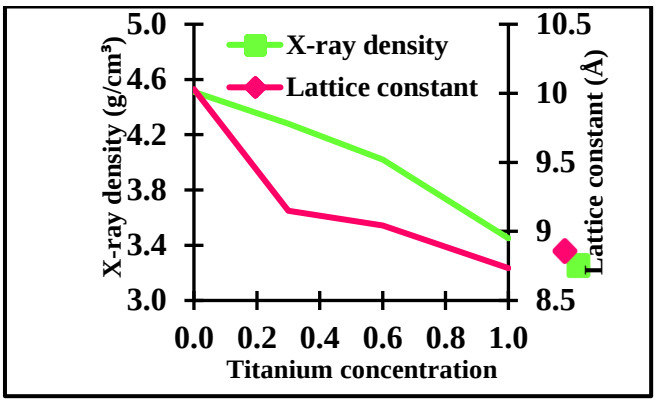

Figure S1. Variation of XRD density lattice constant and XRD density with increasing Ti content.

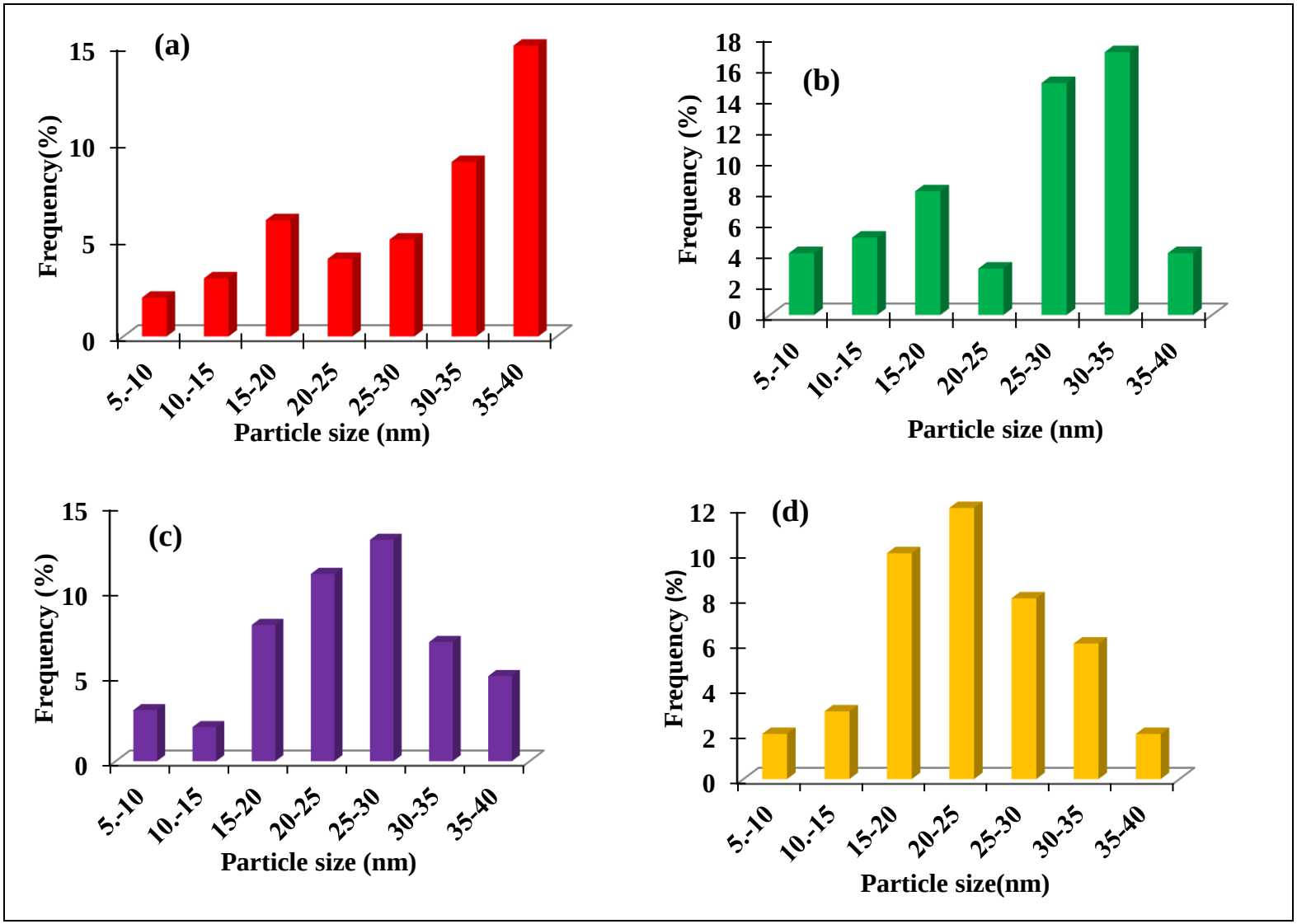

Figure S2. Histograms showing particle size distribution of (a) $SrFe_2O_4$, (b) $TiFe_2O_5$, (c) $Sr_{0.7}Ti_{0.3}Fe_2O_{4.3}$ and (d) Sr0.4Ti0.6Fe2O4.6 NPs**.**

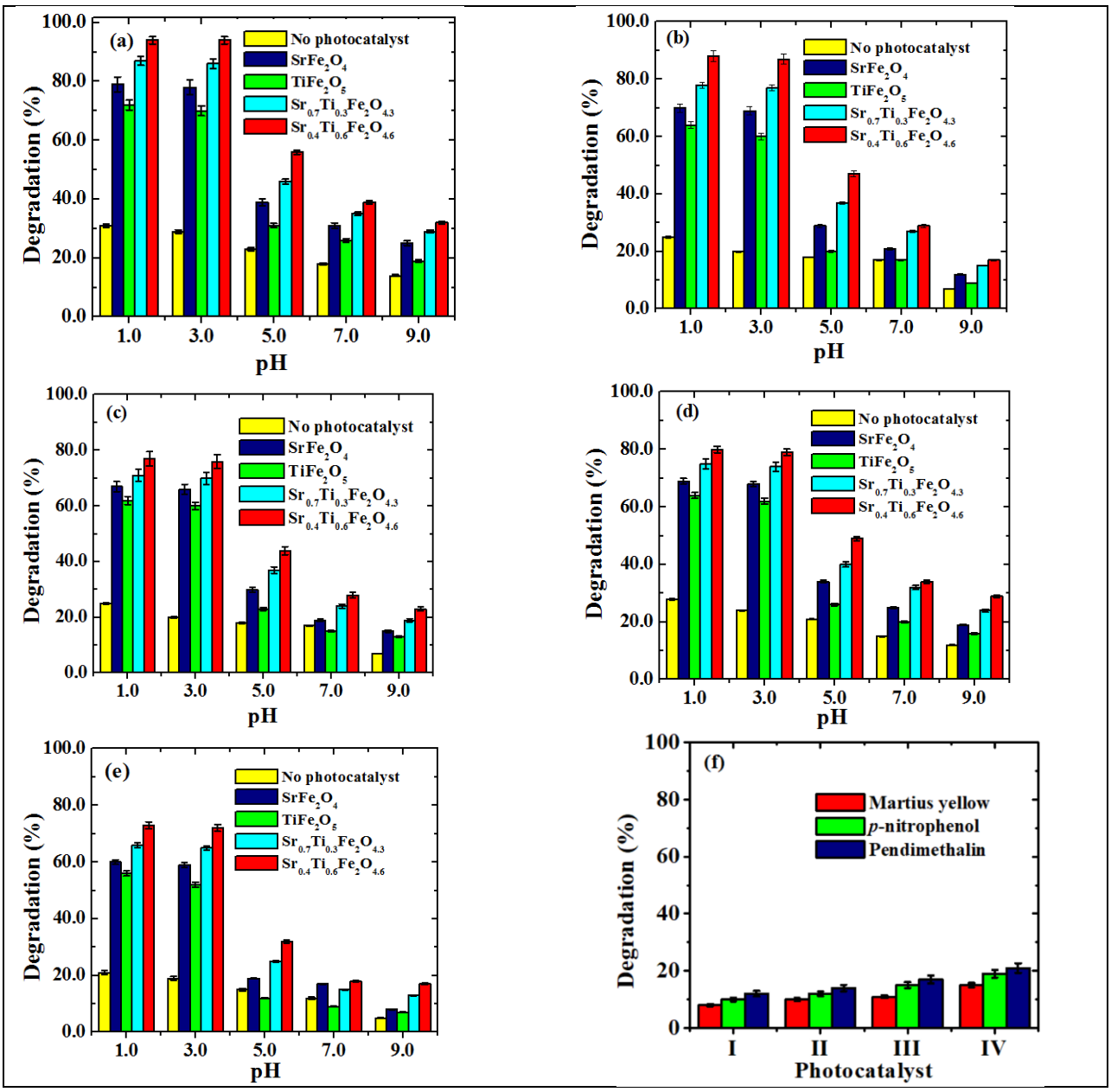

Figure S3. Photocatalytic degradation of (a) pendimethalin and (b) martius yellow under visible light irradiation and (c) *p*-nitrophenol, (d) pendimethalin and (c) martius yellow under ultraviolet light irradiation without catalyst, $SrFe_2O_4$, $TiFe_2O_5$, $Sr_{0.7}Ti_{0.3}Fe_2O_{4.3}$ and $Sr_{0.4}Ti_{0.6}Fe_2O_{4.6}$ NPs(Experimental conditions: catalyst dose, 0.2 g/L for *p*-nitrophenol and pendimethalin, 0.4 g/L for martius yellow; irradiation time, 2 hours and concentration 0.5 mg/L (*p*-nitrophenol and pendimethalin) and 0.05 mg/L (Martius yellow); (f) Photocatalytic degradation of *p*-nitrophenol, pendimethalin and martius yellow without light irradiation using (I) $SrFe_2O_4$, (II) $TiFe_2O_5$, (III) $Sr_{0.7}Ti_{0.3}Fe_2O_{4.3}$ and (IV) $Sr_{0.4}Ti_{0.6}Fe_2O_{4.6}$ NPs (Experimental conditions: catalyst dose, 0.2 g/L for *p*-nitrophenol and pendimethalin, 0.4 g/L for martius yellow; pH, 3.0; irradiation time, 2 hours and concentration 0.5 mg/L (*p*-nitrophenol and pendimethalin) and 0.05 mg/L (Martius yellow).

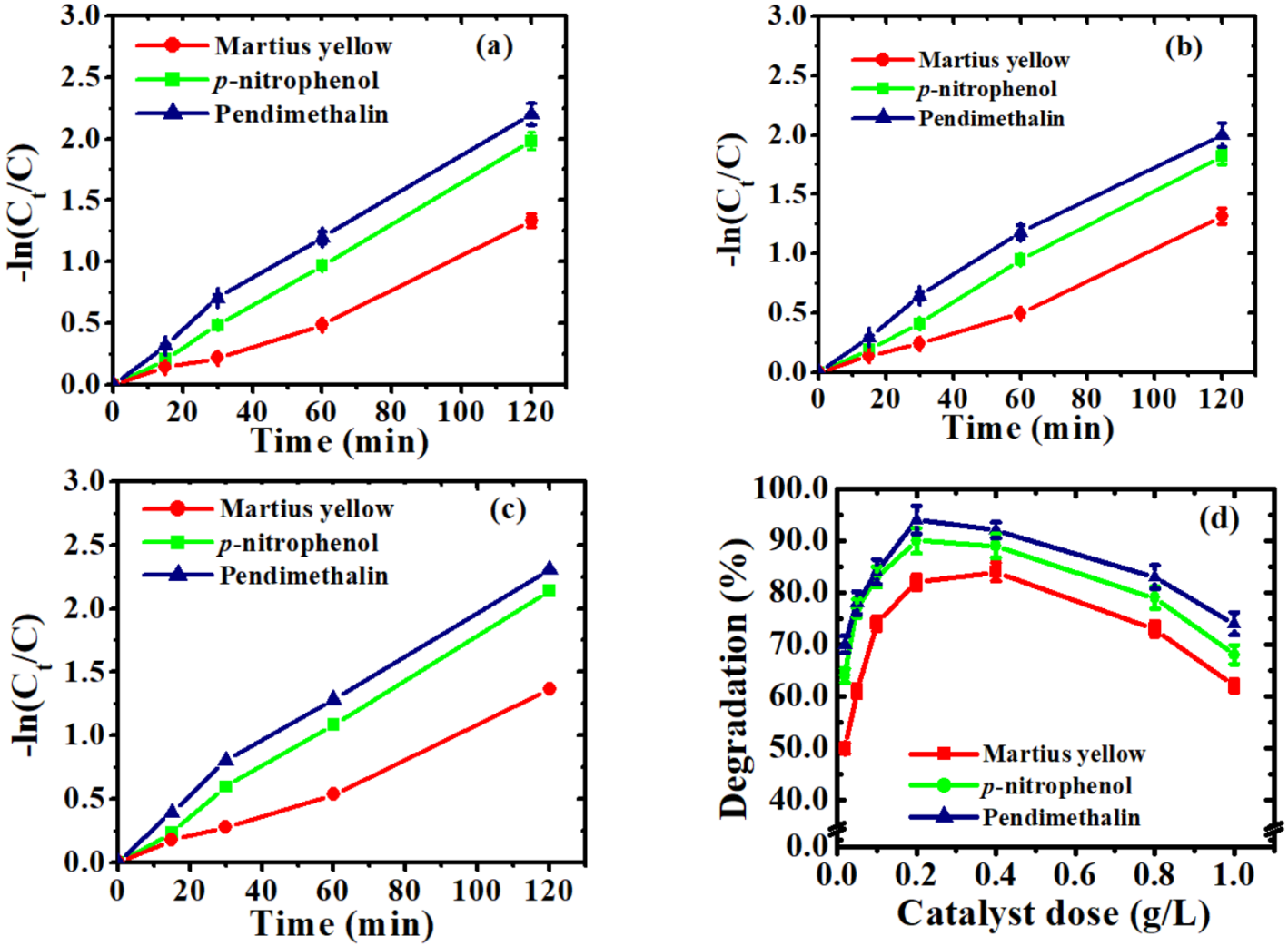

Figure S4. Langmuir-Hinshelwood kinetic plots on photodegradation of nitroaromatic pollutants using (a) $SrFe_2O_4$, (b) $TiFe_2O_5$ and (c) $Sr_{0.7}Ti_{0.3}Fe_2O_{4.3}$ and (d) effect of catalyst dose dose (Experimental conditions: pH, 3.0; irradiation time, 2 hours and concentration 0.5 mg/L (*p*-nitrophenol and pendimethalin and 0.05 mg/L (martius yellow))

Reference:

[35] Lu, C.; Niu, B.; Yi, W.; Ji, Y.; Xu, B. Efficient symmetrical electrodes of $PrBaFe_{2-x}Co_xO_{5+\delta}$ (x = 0, 0.2,0.4) for solid oxide fuel cells and solid oxide electrolysis cells. *Electrochemica Acta*. **2020**, *358*, 136916.